Research Article

Journal of RAMAN SPECTROSCOPY

Received: 10 December 2009 Accepted: 28 February 2010 Published online in Wiley Online Library: 20 April 2010

(wileyonlinelibrary.com) DOI 10.1002/jrs.2661

A comparative study of surface-enhanced Raman scattering from silver-coated anodic aluminum oxide and porous silicon

S. N. Terekhov,[a]* P. Mojzes,[b] S. M. Kachan,[c] N. I. Mukhurov,[a] S. P. Zhvavyi,[a] A. Yu. Panarin,[a] I. A. Khodasevich,[a] V. A. Orlovich,[a] A. Thorel,[d] F. Grillon[d] and P.-Y. Turpin[e]

Three types of Ag-coated arrays from porous anodic aluminum oxide (AAO) were prepared and studied as substrates for surface-enhanced Raman scattering (SERS). They were compared with Ag-coated porous silicon (PSi) samples. AAO-based substrates were prepared by the vapor deposition of silver directly onto the surface of porous AAO with different morphologies of the pores, whereas SERS-active island films on the PSi were prepared by immersion plating. The resulting metallic nanostructures were characterized by UV-vis absorption spectroscopy and scanning electron microscopy (SEM). Thermal evaporation leads to the formation of granular arrays of Ag nanoparticles on the surface of AAO. SERS activity of the substrates was tested using water-soluble cationic Zn(II)-*tetrakis* (4-*N*-methylpyridyl) porphyrin (ZnTMPyP4) as a probe molecule. The results indicate that all AAO-based substrates studied here exhibit some degree of SERS activity. Noteworthy, for excitation at 532 nm, signals from AAO-based substrates were comparable with those from the PSi-based ones, whereas for 441.6 nm excitation they were about twice higher. The strongest SERS-enhancement at 441.6 nm excitationwas provided by the AAO substrates with silver deposited on the monolith (originally nonporous) side of AAO. Preferential SERS-enhancement of the bands ascribed to the vibrations of the *N*-methylpyridinium group of ZnTMPyP4 when going to blue excitation was found.

Keywords: SERS; anodic aluminum oxide; porous silicon; porphyrin

Introduction

Surface-enhanced Raman scattering (SERS) spectroscopy has attracted great attention because of enormous enhancement of Raman signal from molecules adsorbed on noble-metal surfaces exhibiting nanoscale roughness.[1–3] Since enhancements on the order of 10^3–10^6 can be obtained routinely, SERS has become a powerful spectroscopic tool for detection, identification, quantification and structural studies of minute amounts of samples in materials research,[4,5] electrochemistry,[6] surface science,[7] medical diagnostics and biology,[1,8–11] etc. Moreover, under special conditions, enhancement factors up to 10^{10}–10^{15} can be achieved,[2] pushing concentration limits back to the level of a single molecule.[12,13] Due to fluorescence quenching near a metal surface, SERS could be a perfect method of obtaining Raman spectra from strongly fluorescent compounds.

Two different mechanisms take part in the SERS enhancement: (1) the electromagnetic mechanism (EM) resulting from strong enhancement of local electromagnetic field near nanostructured metal surfaces,[14] and (2) the chemical enhancement (CE) arising from electronic resonance/charge transfer between the adsorbed molecule and the metal surface.[15] For a particular analyte, specific nanostructures with tailored properties can be designed to obtain strongly enhanced Raman signals. However, routine employment of the SERS methods for a wide range of analytes requires more versatile substrates that should be reproducible in preparation and response, stable during extended storage, inexpensive and easy to make.

From the early days of SERS history up to the present, the most commonly used SERS-active materials were aggregated Ag and Au colloids[16,17] and roughened electrodes.[18,19] Although aggregated colloids can be easily prepared and often provide strong Raman enhancement, their generally low stability and reproducibility substantially restrict their utility for routine analytical purposes. Silver electrodes, even though more stable and reproducible than colloids, are less sensitive and unhandy for many applications. Feverish search for SERS-active materials with specific properties has resulted in the design and characterization of numerous substrates. Hitherto, more than 100 different SERS-active substrates have been reported. Particu-

* *Correspondence to: S. N. Terekhov, B. I. Stepanov Institute of Physics, National Academy of Science of Belarus, Nezalezhnasti Ave., 70, 220072 Minsk, Belarus. E-mail: terekhov@imaph.bas-net.by*

a *B. I. Stepanov Institute of Physics, National Academy of Science of Belarus, 70, 220072 Minsk, Belarus*

b *Institute of Physics, Faculty of Mathematics and Physics, Charles University in Prague, Prague 2, CZ-12116, Czech Republic*

c *Department of Information Technologies and Robotics, Belarusian National Technical University, 220013 Minsk, Belarus*

d *Centre des Matériaux, Ecole des Mines de Paris, Evry 91030, France*

e *Pierre & Marie Curie University, BioMoCeTi, GENOPOLE Campus 1, 91030 EVRY Cedex, France*

Journal of RAMAN SPECTROSCOPY

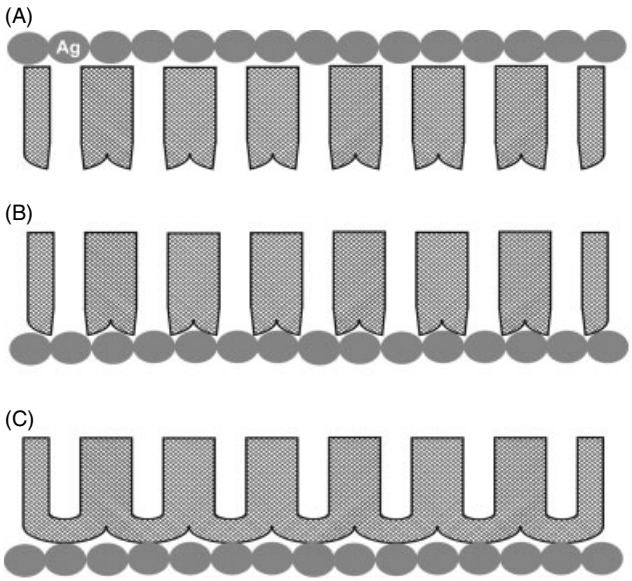

Figure 1. Schematic representation of SERS-active Ag-AAO substrates.

larly, a large number of them have appeared during the last decade due to progress in nanosciences and nanotechnologies. Numerous approaches have been employed to fabricate SERS-active substrates using vapor deposition,[20,21] silver-films-over-nanospheres (AgFONs) coatings,[20] laser ablation,[22,23] cluster formation,[24,25] self-assembly of nanoparticle arrays,[26,27] electron beam lithography,[28] scanning tunneling microscope (STM)-assisted nanostructure formation,[29] nanosphere lithography,[30,31] aggregation of gold nanorods,[32] formation of silver nanowire monolayers,[33] etc.

In general, porous anodic aluminum oxide (AAO), characterized by a closely packed regular array of columnar cells, is a well-established and widely used material for formation of SERS-active nanostructures.[34,35] Pore diameters and pore densities of AAO can be finely controlled, providing a highly ordered matrix into which various metals can be embedded. By filling the AAO pores using electrochemical or metal-vapor deposition techniques, transition-metal nanowire structures,[36] plasmon-resonant Au nanospheres and nanorods with different aspect ratios[37] or noble-metal nanowire arrays exhibiting strong SERS activity[38,39] have been fabricated. A simple method to form a three-dimensional nanocanal arrays with their inner walls coated with Au and Ag nanoparticles based on AAO templates has been recently reported.[40,41] These porous substrates are promising candidates for SERS considering the high surface area for binding the probing molecules, minimal light absorption and scattering and extra enhancement of signal in AAO due to the optical waveguide effect of the pore arrays.[40] According to Ref. [43], promising two-dimensional SERS-active substrates can be prepared by vacuum deposition of silver onto commercially available alumina filters with open pores of 200–300 nm diameter. Surprisingly, in this case the metal deposition was found not to occlude the pores, retaining the filtering abilities of the alumina substrates.[43] However, since the metal was deposited only at the cell partitions, the SERS-active surface was relatively small.

Recently, it has been shown that nonwetting Pb and Sn films thermally evaporated onto AAO substrates spontaneously form ordered nanocrystal arrays in registry with the holes (i.e. they form the negative of the substrate) via grain coalescence.[44] On the other hand, metals that wet the substrate (Pd, Ge) or whose grains do not coalesce at the substrate temperature (Au) do not form such kind of arrays. We have launched a study to test the possibility of engineering Ag-based SERS-active nanostructures in a similar way, by evaporating silver onto one of the surfaces of the AAO substrate. It should be remembered that apart from the obverse porous side, metal can be deposited at the reverse, i.e. monolith, side of the AAO substrate, from which the pores are sealed by a thin hemispherical AAO layer (here called 'a barrier layer'). Additionally, the barrier layer can be removed and the AAO substrate with unsealed pores can be obtained. Thus, by tailoring morphology and, consequently, surface properties of the AAO substrates, different nanoparticle arrays can be prepared by Ag evaporation.

In the present study, three types of SERS-active substrates were fabricated by evaporation of silver onto: the porous side with open pores **(A)**; the monolith side with open pores **(B)**; the monolith side with continuous barrier layer **(C)**. Schematic structures of the Ag–AAO arrays employed here are presented in Fig. 1. To assess SERS activity of these substrates, water-soluble cationic Zn(II)-*tetrakis*(4-*N*-methylpyridyl) porphyrin (ZnTMPyP4) was used as a probe molecule. Various porphyrin and metalloporphyrin derivatives are frequently used as probing analytes for SERS spectroscopy because of their well-assigned Raman spectra, relative photostability, possibility to tailor their photophysical properties by central metal atom and by peripheral substituents as well as the biological importance of some porphyrin derivatives constituting prosthetic groups of enzymes.

There is a problem of accurate quantitative comparison of the SERS enhancement between different kinds of substrates. Precisely, SERS enhancement is to be quantified by the enhancement factor (EF), which is given by the ratio between Raman signal provided by the same number of target molecules exposed to the SERS-active and the SERS-inactive environment of the same state, other experimental conditions remaining exactly the same. Often, for practical reasons, SERS signals from solid surfaces are compared with the normal Raman scattering from solutions. However, even when comparing signals from surfaces, because of the extremely low concentration of analytes used in the SERS experiments, there is a problem of checking the actual number of target molecules involved. Another complication stems from the different analytes and excitation wavelengths used for EF evaluation because of resonance Raman effect. All these factors give rise to considerable uncertainty of the EF evaluation.

To rate potential usefulness of various AAO substrates studied here, their SERS activities were related to another solid-state SERS-active system based on silvered porous silicon (Ag-PSi) prepared by the immersion-plating procedure.[45] Because of their relatively simple preparation, stability in air and compact size, Ag-PSi substrates have become useful SERS-active materials exhibiting several advantages over aqueous silver colloidal systems. We have optimized the preparation of the Ag-PSi substrates to maximize their enhancement for tetrapyrrolic molecules,[46] in particular, for detection of trace amounts of photosensitizer chlorin e_6.[47] Recently, we have investigated SERS on silver-coated mesoporous silicon and estimated the enhancement factor for rhodamine 6G.[48]

Experimental

Chemicals

Cationic ZnTMPyP4 was synthesized according to standard procedures[49] by Dr V. L. Malinovskii (Bogatsky Physico-Chemical Institute, Odessa, Ukraine). Hydrochloric acid (48%) and $AgNO_3$ (>99%) were purchased from Sigma-Aldrich Co. and used without further purification.

Preparation of AAO-based SERS substrates

The AAO films with uniform and parallel nanoporous structure were prepared in a two-step electrochemical anodization process.[50] Aluminum foils with purity of 99.99% were used as the starting material. Before anodization, the aluminum foils were cleaned, degreased and annealed. Anodization was carried out in 4% oxalic acid at a constant current density 3 A dm^{-2} for 60 min. By this procedure, AAO films with a pore diameter of 40 ± 5 nm and average interpore spacing of 120 ± 20 nm were obtained. Unsealing of the barrier layer was carried out by switching on a voltage 1.5 times greater than the final value used for anodization. The arrays of silver nanoparticles in the structures **(A)–(C)** were formed by thermal evaporation of silver onto an AAO substrate of 60 μm thickness at room temperature. The thickness of silver film estimated from deposited mass was about 150 nm.

Preparation of PSi-based SERS substrates

The starting wafers for the preparation of the PSi substrates were p-type, boron-doped, 10 Ω·cm resistivity, (111) orientation silicon crystals. PSi was prepared by electrochemical anodization in a 3 : 1 mixture of HF and ethanol. The anodic current density and time of anodization were 20 mA cm^{-2} and 30 min, correspondingly.

Silver deposition was carried out by the immersion-plating method from an aqueous solution of $AgNO_3$. Before the deposition procedure, PSi plates were rinsed for several seconds in an aqueous HF : ethanol mixture to remove a layer of the oxidized silicon. Then samples were thoroughly rinsed with ethanol and water. After these initial steps, PSi plates were placed into 10 mM water solution of $AgNO_3$ for 10 min followed by rinsing with ethanol, and then dried. To eliminate contaminants adsorbed on the nanostructured silver surface, which often give rise to rather strong SERS background, the Ag-PSi substrates were immersed into a 10 mM HCl solution for several seconds.

Spectroscopic measurements

UV-vis and luminescence

UV-vis reflection and absorption spectra were recorded on Cary 500 Scan (Varian) spectrophotometer. The photoluminescence measurements were conducted with a spectrofluorometer SDL 2, equipped with a photomultiplier sensitive in the 230–800 nm region.

Surface-enhanced Raman scattering

Both AAO-based and PSi-based samples for SERS measurements were prepared by immersion of the substrates in identical aqueous porphyrin solutions (3 ml) of 10^{-6} M for a 1.5 h. In principle, such analyte deposition could result in different surface concentrations for various substrates due to their possible differences in adsorption abilities. However, as the SERS signal comes mainly from the molecules occupying the 'hot spots' rather than from all the molecules attached to the surface, and taking into account enhanced affinity of the analyte to the hot spots,[51] the prolonged immersion (1.5 h) ensures saturation of the active sites to provide maximal SERS activity of the substrates.

To compare the SERS activity of the AAO- and PSi-based substrates, Raman spectra were recorded using a Spectra Pro 500 I spectrometer (180° backscattering geometry of excitation), a homemade Raman spectrometer equipped with a liquid-nitrogen-cooled CCD detector Spec-10 : 256 (Roper Scientific, USA) and a multichannel Raman spectrometer based on a Spex 270M (Jobin Yvon) spectrograph and liquid-nitrogen-cooled CCD detector (Princeton Instruments). Spectra were excited by the wavelengths 441.6 nm (He–Cd laser); 457.9, 488.0 and 514.5 nm (Ar^+ laser); and 532.0 nm (continuous diode-pumped Nd : YAG laser).

Excitation profiles of relative enhancement factors (REF) were determined from the SERS spectra of ZnTMPyP4 adsorbed on the Ag-coated AAO, obtained at typically 10–40 mW power focused on to the sample (laser spot diameter ~100 μm). The same experimental conditions as well as identical scattering geometries (90° laser beam-to-collecting optics arrangement; 57° normal of the sample surface-to-laser beam orientation) were used for all excitation wavelengths. For each excitation, 10 SERS spectra were collected from different spots inside a restricted area (~4 mm^2) to average out possible inhomogeneities of the sample. SERS intensities were reciprocally normalized using the nonresonant Raman spectrum of glass (broad band at ~1095 cm^{-1}) from the microscopic slide supporting the sample as an external intensity standard. For each excitation, 10 spectra of the glass standard were taken under identical experimental conditions, laser power and scattering geometry as the SERS spectra of the sample.

Results and Discussion

SEM characterization of AAO- and PSi-based SERS substrates

Scanning electron microscopy (SEM) images of the Ag-AAO and Ag-PSi samples are shown in Figs 2 and 3, respectively. As can be seen from the SEM images, thermal evaporation leads to the formation of granular silver films (arrays of nanoparticles) on the surface of the AAO substrate. Topologies of the silver films strongly depend on the morphology of porous substrates and are qualitatively different for all samples. The analysis of the SEM images was performed with a self-made software which approximated each nanoparticle as an ellipse with the same normalized second central moments as the nanoparticle surface. On the right panels of Fig. 2, we present statistical distributions of the minimal lengths (minor axes) and maximal lengths (major axes) of such equivalent ellipses for all the Ag-AAO samples.

The most regular array of silver nanoparticles is exhibited by the sample **(A)**. The regularity of this structure reflects the regularity of pores in the underlying AAO substrate: centers of individual nanoparticles are located exactly at the pore sites. As seen from both the SEM image and the size distribution histograms, three types of nanoparticles can be distinguished in this sample. Most of the nanoparticles (~47%) are slightly elliptical with the average minimal length of 65 ± 9 nm and average maximal length of 78 ± 11 nm. However, some of the such sphere-like nanoparticles are coalesced with the neighbors into two- or three-nanoparticle clusters. The coalesced pairs constitute around 41% of the total number of the particles and are characterized by the maximal length of 138 ± 20 nm. The remaining

Journal of RAMAN SPECTROSCOPY

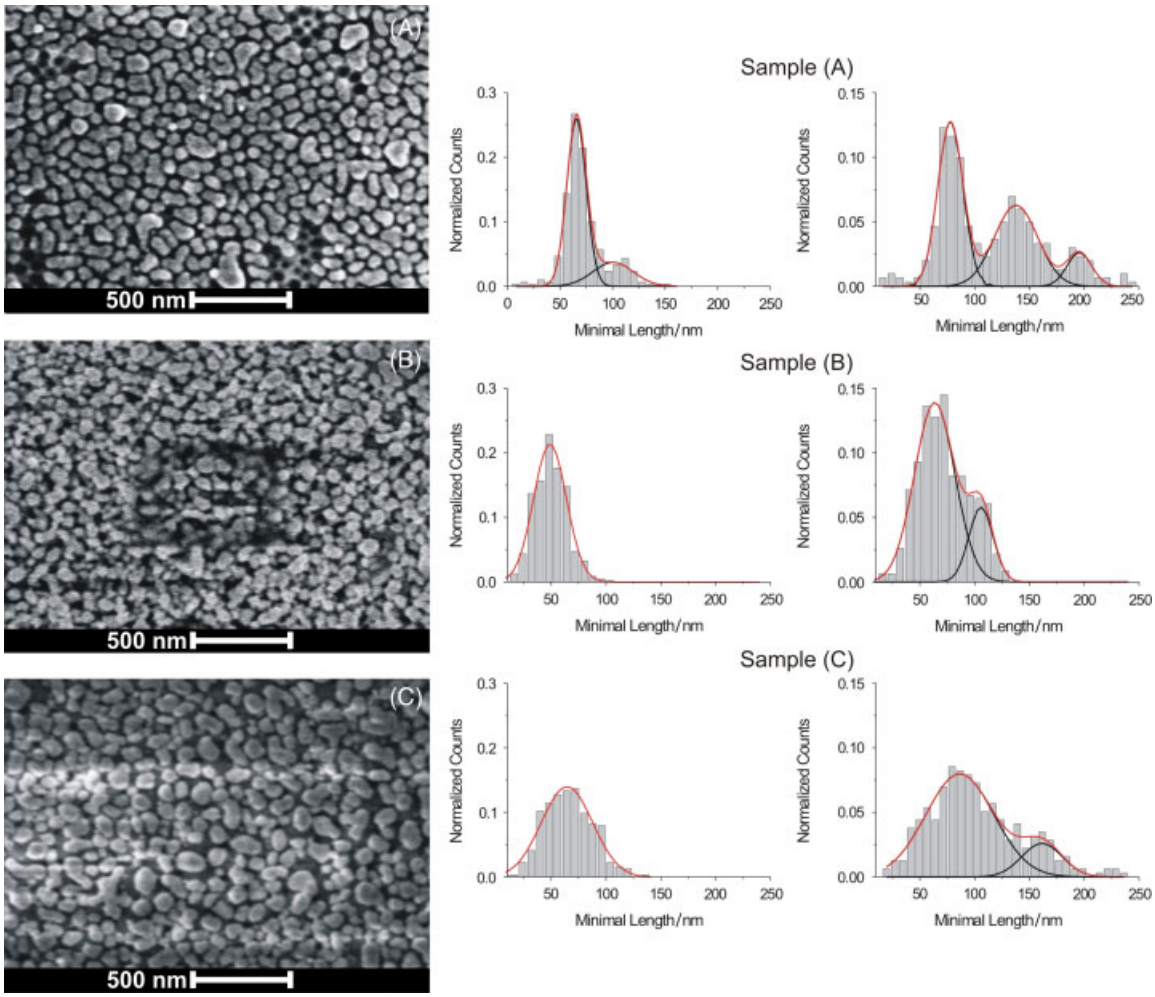

Figure 2. SEM images of nanoparticle arrays (left panel) and histograms of the nanoparticles' minimal and maximal lengths (i.e. minor and major axes of effective ellipsoids) fitted by Gaussian distributions (right panel) for the Ag-AAO samples.

particles (∼12%) can be considered as conglomerates of three and more 'base' particles. Among them, one should distinguish highly elliptical chain-like particles and triples of neighboring particles, which are responsible for the second peak (100 ± 19 nm) in the minimal length distribution. Due to high regularity of the structure **(A)**, it is characterized by a very small number of almost touching particles – most of them are sharply separated from each other. This weakens the plasmon coupling in such structures and, therefore, prevents the emergence of strong local field enhancement areas (hot spots) required for the SERS.

The least regular structure **(B)** consists of small particles with a minimal length of ∼49±15 nm and maximal length of ∼63±18 nm and tend to aggregate into fractal-like clusters. Many of them are touching each other; therefore resolution of the individual particles and statistical analysis of this structure was quite ambiguous. In contrast to the structure **(A)**, the existence of many almost touching particles should facilitate the appearance of hot spots. However, a percolation due to the multitude of closely located touching particles (with good electric conductance between them) is expected to significantly weaken this effect.

The structure **(C)** is intermediate between the structures **(A)** and **(B)**. In contrast to structure **(B)**, it consists of well-separated nonpercolating particles. At the same time, in contrast to structure **(A)**, this structure is not so regular: its essentially elliptical particles (with minimal length of ∼65 ± 24 nm and maximal lengths of ∼87 ± 31 nm and ∼160 ± 18 nm) have a much broader size distribution. The distance between neighboring particles exhibits also significant variations; many of the particles are almost touching each other, resulting in strong local field enhancement in such areas.

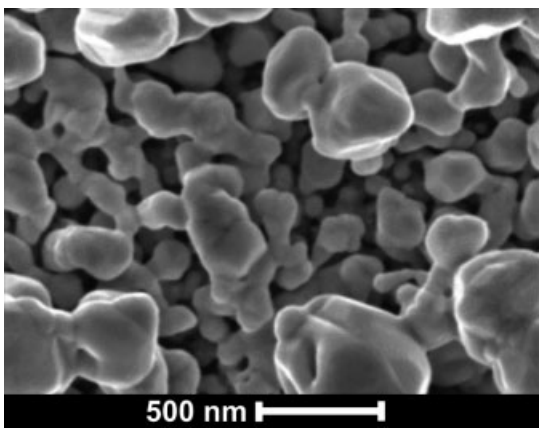

Figure 3. SEM image of the nanoparticle array for the Ag-PSi sample.

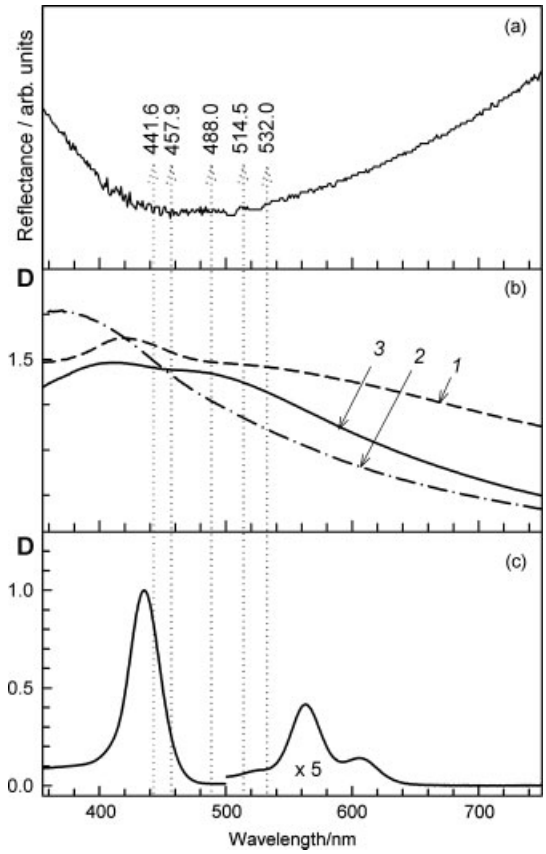

Figure 4. Reflectance spectrum of Ag-coated PSi (a); Extinction spectra of Ag-AAO substrates (b): 1 – structure **(A)**; 2 – structure **(B)**; 3 – structure **(C)**; Optical absorption spectrum of ZnTMpyP4 in water solution (c).

The structure of discontinuous silver film at the surface of Ag-PSi sample (Fig. 3) seems to consist of several layers of particles with various diameters. The ground layer is a conglomerate of coalescent particles with the size of around 80 nm. It is covered by large individual particles with the size reaching 550–600 nm. The complex topology of such a structure does not permit any statistical analysis. From qualitative consideration, it can be expected that the Ag-PSi substrate should provide moderate field enhancement in broad spectral range of excitation.

UV-vis spectra

UV-vis absorption spectra of Ag-AAO structures **(A)**–**(C)**, the reflectance spectrum of Ag-PSi and the absorption spectrum of ZnTMPyP4 in aqueous solution are shown in Fig. 4. For the convenience of further analysis of SERS activity, the wavelengths of laser excitations used here are depicted by vertical dotted lines. The absorption spectra of all Ag-AAO samples, corrected for intrinsic absorbance of the aluminum oxide substrate, exhibit pronounced surface plasmon bands (Fig. 4(b)), however, with different positions and shapes. Specifically, the spectrum of structure **(A)** has a distinct maximum near 420 nm and an additional broad excitation near 550 nm. Structure **(C)** also displays a dual peak centered near 410 and 480 nm, but in contrast to sample **(A)** their strengths are not very different from each other. Finally, sample **(B)** is characterized by only a single absorbance peak near 380 nm.

Taking into account that the resonant wavelength of plasmon excitation increases with the nanoparticle size, one can notice good correlation between the absorption spectra and nanoparticle size distributions for the samples **(A)**–**(C)** (Fig. 2). Indeed, samples **(A)** and **(C)** consist of nanoparticles with multimodal size distributions and, thus, in addition to nearly spherical particles with size around 65–85 nm, they contain essentially a large fraction of highly elliptical nanoparticles with maximal length exceeding 130 nm. Evidently, this multimodal size distribution should manifest itself in a multiband structure of the plasmon absorbance. Therefore, the long-wavelength peaks of samples **(A)** and **(C)** can be attributed to the plasmon excitations in the large-size, highly elliptical particles. The slow decay of the long-wavelength tail of plasmon band of sample **(A)** [when compared with the sample **(C)**] as well as its red shift should be caused by the notable presence of large nanoparticles with sizes around 200 nm. Besides, the strong quadrupole modes of such large nanoparticles appearing at wavelengths close to dipole resonances of small nanoparticles can contribute to the plasmon peak of sample **(A)** at 410 nm, making it more pronounced than in sample **(C)**. The blue shift of the surface plasmon band for sample **(B)** in comparison with samples **(A)** and **(C)** can be explained by the much smaller average size of nanoparticles in sample **(B)**.

Considering the reflection spectrum of the Ag-PSi substrate (Fig. 4(a)) over the spectral range studied, its surface plasmon resonance appears as a broad, structureless band with a minimum centered at 500 nm, in accord with the wide size distribution of Ag nanoparticles.

SERS activity

Our spectral measurements revealed that all the AAO-based substrates exhibit considerable SERS activity when using ZnTMPyP4 (1×10^{-6} M) as the analyte. In contrast, no SERS signal was observed when this porphyrin was adsorbed from the solution of the same concentration on the Ag film vacuum-deposited on a flat aluminum mirror. To relate the enhancement of the Raman signal to the plasmon resonances of the Ag-AAO substrates, the SERS excitation profiles were measured (Fig. 5). Integrated SERS intensities of the most intense Raman bands (1353, 1553 and 1638 cm^{-1}) were normalized with respect to the glass band at ~1095 cm^{-1} used as intensity standard (see Experimental section), so that the SERS profiles are presented as REFs taking the SERS intensity of sample **(A)** excited by 532.0 nm as a unit.

It can be seen from Fig. 5 that the SERS enhancement for all three structures is much larger at blue excitation, being enhanced 10–12 times when going from 532.0 to 441.6 nm. Since excitation profiles seem to follow the absorption curve of ZnTMPyP4 (Fig. 4(c)), one can presume that the observed behavior of the SERS profiles is mainly due to the resonance contribution of the analyte to surface-enhanced resonance Raman scattering (SERRS). Actually, the absorption spectrum of ZnTMPyP4 consists of strong electronic transition at 435 nm corresponding to the Soret band and two rather weak Q-bands located at 563 and 606 nm; therefore, one can expect that excitation at 441.6 nm should be more favorable than those at larger wavelengths. However, our results presented in Fig. 6 contradict this explanation.

Figure 6 compares in detail the 532 and 441.6 nm excited SERS spectra of ZnTMPyP4 adsorbed from solutions with identical concentration (1×10^{-6} M) on the Ag-AAO sample **(A)** and the Ag-PSi substrate. Sample **(A)** was chosen because of the smaller fluorescence background compared to the samples **(B)** and **(C)**. As

Journal of RAMAN SPECTROSCOPY

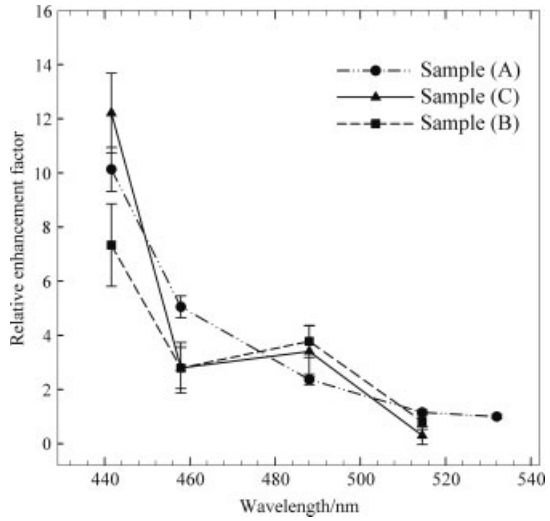

Figure 5. Dependence of the relative enhancement factor for the Ag-AAO samples **(A)**–**(C)** on the excitation wavelength.

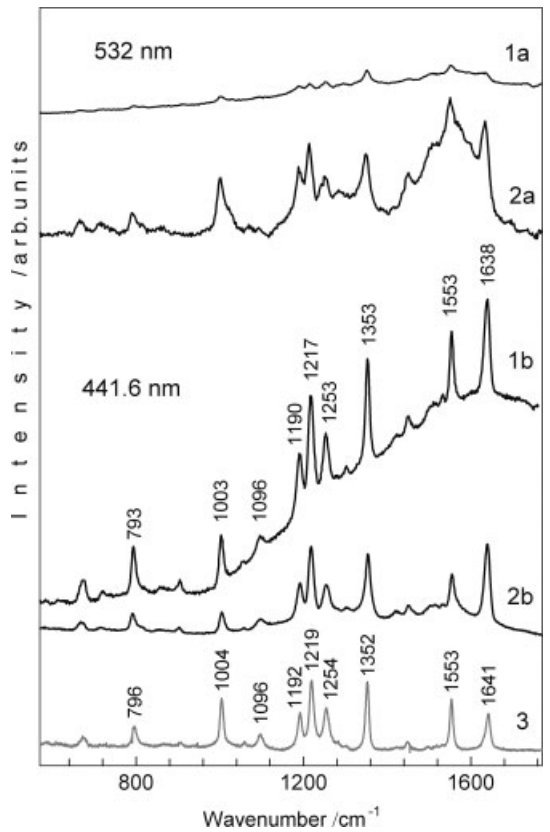

Figure 6. SERS spectra of ZnTMpyP4 (10^{-6} M) adsorbed on silvered surface of AAO (1a, 1b) and PSi (2a, 2b). Resonance Raman spectrum of ZnTMpyP4 (10^{-4} M) water solution. Spectra were taken at 532 nm (1a, 2a) and 441.6 nm (1b, 2b, 3).

seen from Fig. 6, when excited at 441.6 nm, the Ag-AAO substrate **(A)** exhibits about twice greater enhancement compared to that of the Ag-PSi substrate. However, when excited at 532 nm, the SERS intensity from the Ag-PSi is about six times stronger than that from the Ag-AAO **(A)**. At the same time, plasmon absorbances (reflectances) of the Ag-PSi at 441.6 and 532.0 nm are nearly equal, similar to the SERS enhancements for the corresponding excitations (data not shown). Thus, it can be suggested that the SERS enhancement of the AAO-based substrates is governed by the resonance with their surface plasmons rather than with the electronic absorption of the analyte.

It is commonly known[14,52] that SERS is closely related to the local field enhancement due to plasmon excitations. As is also known, such local field enhancement is mostly pronounced near the surface of small-sized nanoparticles, whose plasmon resonances are located in the shorter wavelength region. Since all three Ag-AAO substrates contain a large fraction of relatively small nanoparticles, this can qualitatively explain why their SERS enhancements are greater for the blue excitation and rapidly decay with increasing wavelength. Moreover, this also explains why the SERS intensity for the Ag-PSi sample is almost independent of the excitation wavelength. Indeed, nanoparticles at the surface of Ag-PSi accessible for the analyte are of very large sizes (reaching 500–600 nm, Fig. 3) and, therefore, the plasmon-induced local fields associated with them remain relatively weak for all wavelengths in the visible range.

Let us compare the SERS activities of the different Ag-AAO substrates in detail. Though the general trends in their SERS profiles are similar (SERS intensity decaying with increasing wavelength), the exact forms of their REF dependences are different (Fig. 5). For example, at 441.6 nm the maximum of the SERS intensity is observed for structure **(C)**, whereas at 457.9 nm it is for structure **(A)**. Moreover, several intersections can be found in the SERS profiles. Thus, in principle, it makes no sense to compare the absolute SERS enhancements of different Ag-AAO substrates as an *ipso facto*, since their SERS activities depend on particular excitation conditions.

For 441.6 nm excitation, the shortest wavelength used here, for which the REFs reached their largest values, the difference between the SERS intensities for the three Ag-AAO substrates could be explained from the viewpoint of the existence of delocalized plasmon states in such silver structures. Indeed, theoretical[53] and experimental[54] investigations of random metal–dielectric films have revealed that excitation of delocalized surface plasmon modes leads to reduction in the local field fluctuations and minimization of the SERS enhancement at the percolation threshold.

Since the physical origin for the delocalized states lies in the short-range correlations in the spatial distribution of metal conductivity, this effect should be quite general and thus applicable to our systems as well. All our Ag-AAO substrates have different topologies of nanoparticle arrays resulting in different probabilities of existence of delocalized surface plasmon modes. In particular, the array of nanoparticles in substrate **(B)** can be presented as a fractal-like percolation system demonstrating the largest (among the substrates studied here) probability of appearance of delocalized surface plasmon modes. Accordingly, this sample exhibits the smallest SERS intensity with blue excitation. Sample **(A)** also favors to some extent the formation of delocalized surface plasmon modes due to significant spatial correlation between nanoparticles bound to the regularly distributed pore sites. In combination with nanoparticle size disorder, such a spatial ordering leads to only partial delocalization of surface plasmon states and, thus, sample **(A)** has a larger SERS-enhancement factor as compared to sample **(B)**. For sample **(C),** the ensemble of nanoparticles is characterized not only by strong size disorder but also by prominent position disorder, which together

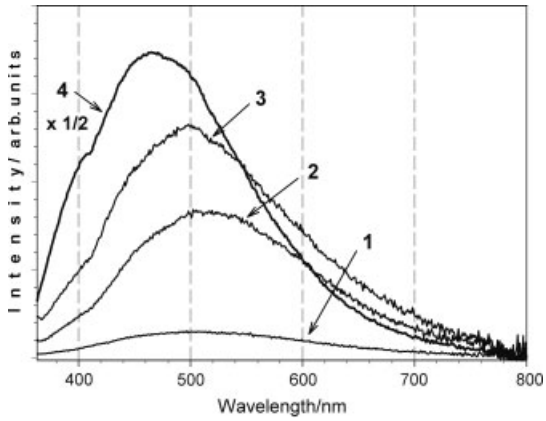

Figure 7. Photoluminescence spectra of Ag-AAO samples **(A), (B), (C)** – curves 1, 2, 3, respectively, and original AAO plate without Ag – 4. Spectra were obtained under 325 nm excitation.

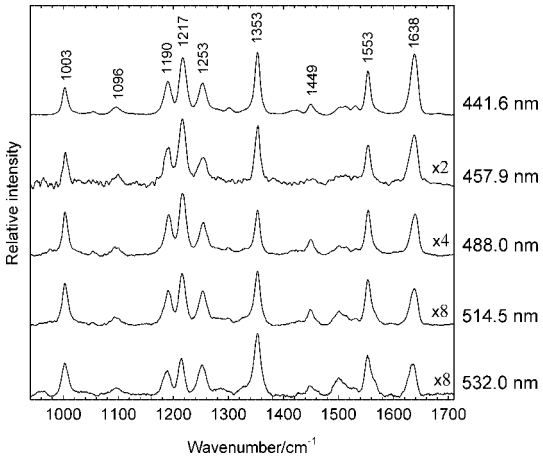

Figure 8. Normalized SERRS spectra of ZnTMPyP4 adsorbed on the Ag-coated AAO obtained by various excitation wavelengths. For clarity, spectra are enlarged correspondingly.

suppress formation of delocalized states and, therefore, provide the largest SERS intensity when excited by 441.6 nm.

Photoluminescence of the AAO-based substrates

AAO-based substrates were found to provide SERS spectra with a rather strong luminescence background. The SERS spectrum from sample **(A)** depicted in Fig. 6 demonstrates minimal level of background among the substrates studied here. To identify the origin of the background, photoluminescence spectra (excitation 325 nm) of the substrates **(A)**–**(C)** were recorded before their imersion in ZnTMpyP4 solution (Fig. 7). For all three Ag-AAO substrates, a broad emission band centered at 500 nm was detected, with the luminescence intensity increasing in the order A < B < C. Evidently, fluorescence background underlying the 441.6 nm SERS spectra is not due to ZnTMpyP4 itself, despite the fact that ZnTMpyP4 in solution exhibits rather strong emission. It is probably related to the intrinsic photoluminescence of the AAO material, since previous investigations of the AAO films formed in oxalic acid solutions have reported photoluminescence with a peak around 470 nm.[55] In fact, as can be seen from Fig. 7, the photoluminescence spectrum of the original AAO film before Ag coating (with continuous barrier layer) obtained by the anodization procedure in the presence of oxalic acid has a strong emission at 470 nm. It is agreed in the literature that oxalic acid impurities incorporated into the AAO plates during anodization are responsible for this emission.[55–57] It is worthwhile to note that the photoluminescence maxima of Ag-coated AAO substrates studied here are centered near 500 nm. We suggest that the absorption of the photoluminescent emission by the nanostructured Ag deposit, more effective at the blue side of the 470 nm band because of stronger plasmon resonance, gives rise to this red shift. As this photoluminescence strongly contributes to Raman spectra of AAO-based substrates, we are going to undertake a special study how to eliminate this effect. The AAO films can be annealed at high temperatures to remove oxalic acid impurities before Ag coating, or other types of electrolytes (e.g. sulfuric and phosphoric acids) can be used for anodization.

Relative enhancement factors for Raman bands of ZnTMpyP4

On measuring the excitation profiles of the Ag-AAO samples, different dependences of the SERS intensities were noticed for various Raman bands of ZnTMPyP4. To investigate this effect in detail, statistically more relevant sets of SERS spectra were taken for the Ag-AAO substrate **(A)** using all the laser lines at our disposal. Structure **(A)** was chosen because of its moderate fluorescence, enabling acquiring the spectra with better signal-to-noise ratio for all excitations. It should be remembered again that only REFs were estimated because the number of ZnTMPyP4 molecules contributing to the SERS signal remained unknown. Typical normalized SERS spectra for each excitation are shown on Fig. 8. For clarity, the displayed spectra were corrected for laser plasma lines and fluorescence background, and rescaled adequately (expanded two to eight times). Even a cursory examination reveals interesting variations in the relative intensities of certain Raman bands when going from 532.0 to 441.6 nm, disclosing existence of two sets of Raman bands exhibiting different REF values.

Integral intensities from peak fitting/decomposition and statistical treatment of datasets were used to obtain reliable average REFs along with their standard deviation errors (Table 1). As seen from dependences of the REF on the excitation wavelength (Figs 9 and 10), bands located at 1190, 1217 and 1638 cm^{-1} were found to be enhanced ~13–16 times when going from 532.0 to 441.6 nm, whereas bands at 1353 and 1553 cm^{-1} attain a factor only ~7–8. The same order of REF shows three more bands of medium intensity at 1003, 1096 and 1253 cm^{-1} (data not shown). A similar effect was reported for ZnTMPyP4 previously[58] when comparing intensities of individual Raman bands in resonance Raman spectra with those of SERS-enhanced in borohydride-reduced Ag colloids. It should be remembered that the overall REF representing weighted mean of the factors obtained for individual bands from the 950–1750 cm^{-1} region reaches ~10 (Fig. 5).

As remarked previously,[58] a common feature of the bands exhibiting stronger enhancement is their assignment to the deformation vibration of the *N*-methylpyridinium group δ(pyr).[59,60] Surprisingly, the strong relative enhancement of the 1638 cm^{-1} band might be thus explained by the enhancement mechanism of the SERS,[61–63] taking into account the orientation of the porphyrin macrocycle relative the silver surface. The analysis of SERS spectra with regard to the orientation of the analyte is based on the surface selection rules founded on the electromagnetic theory of SERS intensities. According to these rules, the greatest enhancement would be experienced by the vibrational modes involving a change in molecular polarizability with the component normal to

Table 1. Relative enhancement factors of ZnTMPyP4 bands as a function of the excitation wavelength

Raman band (cm^{-1})	REF for excitation wavelength					Band assignment[60,61]
	532.0	514.5	488.0	457.9	441.6	
1003	1.0 ± 0.1	1.1 ± 0.1	2.8 ± 0.2	3.7 ± 0.3	7.3 ± 0.5	$\nu_s(C_\alpha C_m)$, A_{1g}
1096	1.0 ± 0.1	1.2 ± 0.1	2.0 ± 0.3	5.1 ± 0.4	7.1 ± 0.7	$\delta_s(C_\beta H)$, A_{1g}
1190	1.0 ± 0.1	1.3 ± 0.2	3.7 ± 0.4	6.2 ± 0.6	12.7 ± 0.9	δ(pyr), $\nu(N^+\text{-}CH_3)$, A_{1g}
1217	1.0 ± 0.1	1.3 ± 0.1	3.3 ± 0.3	7.7 ± 0.7	12.6 ± 0.9	δ(pyr), A_{1g}
1253	1.0 ± 0.1	1.1 ± 0.1	2.0 ± 0.2	3.5 ± 0.3	8.3 ± 1.0	$\nu(C_m\text{-pyr})$, A_{1g}
1353	1.0 ± 0.1	0.8 ± 0.1	1.3 ± 0.1	3.7 ± 0.3	7.3 ± 0.5	$\nu_s(C_\alpha N)$, A_{1g}
1553	1.0 ± 0.1	1.2 ± 0.1	2.0 ± 0.2	3.7 ± 0.4	7.7 ± 0.9	$\nu_s(C_\beta C_\beta + C_\alpha C_m)$, A_{1g}
1638	1.0 ± 0.1	1.3 ± 0.1	2.7 ± 0.3	6.8 ± 0.6	15.9 ± 1.6	δ(pyr), A_{1g}

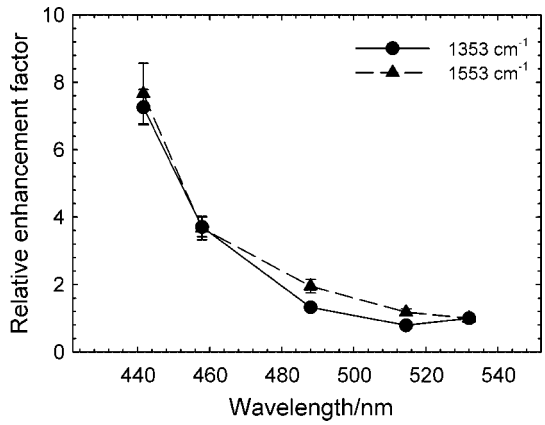

Figure 9. Excitation dependence of the relative enhancement factors for the 1353 and 1553 cm^{-1} bands.

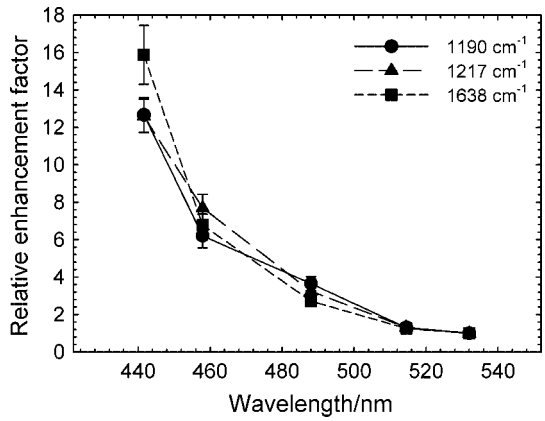

Figure 10. Excitation dependence of the relative enhancement factors for the 1190, 1217 and 1638 cm^{-1} bands.

metal surface, e.g. out-of-plane vibrations for the planar molecule in parallel orientation with respect to the active surface. The space molecular configuration can be deduced from the comparison of normal Raman spectrum with the corresponding SERS spectrum.

Comparing 441.6 nm excited SERS spectra of ZnTMPyP4 with the RRS spectrum in water solution (Fig. 6), the higher relative intensities of two SERS bands peaking at 1638 and 793 cm^{-1} relative to those in RRS spectrum can be observed. Furthermore, though maxima of the bands in SERS spectra coincide closely with those in RRS, the four discussed bands (793, 1190, 1217 and 1638 cm^{-1}) show distinct shifts relative to their ordinary Raman counterparts. A similar comparison for the 532.0 nm excitation cannot be done because of strong fluorescence background and unsuitable resonance conditions of ZnTMPyP4 in solution. It should be noted that all the bands in question are due to the *N*-methylpyridinium vibrations. The analogs of 1638 and 793 cm^{-1} have been recognized as indicators of the orientations of other porphyrins adsorbed on metal surfaces.[64] This implies that interaction between the ZnTMPyP4 molecules and the silver surface takes place via *N*-methylpyridinium groups which are supposed to be attached to the negatively charged metal surface via Coulombic interaction and have near-perpendicular orientation. In such a situation, the porphyrin macrocycle should be parallel to the silver surface. It is noteworthy that SERS spectral features, including the peak positions and relative band intensities, seem to be identical for both AAO- and PSi-based substrates, suggesting similar binding modes. In this connection, it was found recently[65] that the water-soluble H_2TMPyP4 molecules at low concentration lie flat on the Ag surface.

As the electric field decreases exponentially with the distance from the metal surface, vibrations of the porphyrin core would experience additional decrease of Raman enhancement in comparison with those of *N*-methylpyridinium groups. As for the preferred SERS enhancement of the bands ascribed to the *N*-methylpyridinium vibrations by 441.6 nm excitation, it can be suggested that, due to near-perpendicular orientation to the surface, they have to undergo more effective enhancement when the excitation wavelength approaches the maximum of localized plasmon resonance.

Conclusions

Three types of Ag-coated anodic aluminum oxide substrates have been studied. It was shown that silver evaporation onto AAO surface results in the formation of nanostructured arrays appropriate for plasmon propagation. All of the AAO-based substrates exhibited some degree of SERS activity in relation to ZnTMPyP4 used as analyte. Raman enhancement by Ag-AAO substrate was compared with that of Ag-plated PSi: for the excitation at 532 nm, signals from Ag-AAO was comparable to those from PSi, whereas for the 441.6 nm it was about twice higher. It was suggested that the excitation resonance with the plasmon extinction rather than with electronic absorption of the analyte governs the SERS enhancement in the SERS-active AAO-based substrates. Therefore, the relative SERS activity of the Ag-AAO structures has to be compared at distinct excitation conditions.

Acknowledgements

This work was supported by the National Academy of Sciences of Belarus through the Programs 'Fotonika' (Project 3.15), the Belarusian Republican Foundation for Fundamental Research (Project F08-MC011), Ministry of Education of the Czech Republic (MSM0021620835), the Grant Agency of the Charles University in Prague (224/2006/B-Fyz/MFF) and the Grant Agency of the Czech Republic (203/07/0717). We also thank Dr I. V. Gasenkova for providing the AAO samples.

References

[1] R. Aroca, *Surface-Enhanced Vibrational Spectroscopy*, John Wiley & Sons: Chichester, **2006**.
[2] K. Kneipp, H. Kneipp, I. Itzkan, R. R. Dasari, M. S. Feld, *Chem. Rev. (Washington, D.C.)* **1999**, *99*, 2957.
[3] L. A. Lyon, C. D. Keating, A. P. Fox, B. E. Baker, L. He, S. R. Nicewarner, S. P. Mulvaney, M. J. Natan, *Anal. Chem.* **1998**, *70*, 341R.
[4] S. Lefrant, I. Baltog, M. B. Baibarac, *J. Raman Spectrosc.* **2005**, *36*, 676.
[5] L. Li, D. S. Zhou, G. Xue, *J. Raman Spectrosc.* **2005**, *36*, 699.
[6] P. G. Cao, Y. H. Sun, R. N. Gu, *J. Raman Spectrosc.* **2005**, *36*, 725.
[7] A. Campion, P. Kambhampati, *Chem. Soc. Rev.* **1998**, *27*, 241.
[8] S. Cî nta Pî nzaru, I. Pavel, N. Leopold, W. Kiefer, *J. Raman Spectrosc.* **2004**, *35*, 338.
[9] J. M. Reyes-Goddard, H. Barr, N. Stone, *Photodiagnosis Photodyn. Ther.* **2005**, *2*, 223.
[10] J. Kneipp, H. Kneipp, K. Kneipp, *Chem. Soc. Rev.* **2008**, *37*, 1052.
[11] K. Hering, D. Cialla, K. Ackermann, T. Dorfer, R. Moller, H. Schneidewind, R. Mattheis, W. Fritzsche, P. Rosch, J. Popp, *Anal. Bioanal. Chem.* **2008**, *390*, 113.
[12] K. Kneipp, Y. Wang, H. Kneipp, L. T. Perelman, L. Itzkan, R. R. Dasari, M. S. Feld, *Phys. Rev. Lett.* **1997**, *78*, 1667.
[13] S. Nie, S. R. Emory, *Science* **1997**, *275*, 1102.
[14] M. Moskovits, *Rev. Mod. Phys.* **1985**, *57*, 783.
[15] A. Otto, I. Mrozek, H. Grabhorn, W. Akemann, *J. Phys. Condens. Matter* **1992**, *4*, 1143.
[16] P. C. Lee, D. Meisel, *J. Phys. Chem.* **1982**, *86*, 3391.
[17] C. G. Blatchford, J. R. Campbell, J. A. Creighton, *Surf. Sci.* **1982**, *120*, 435.
[18] B. H. Loo, *J. Phys. Chem.* **1983**, *87*, 3003.
[19] Q. J. Huang, J. L. Yao, B. W. Mao, R. A. Gu, Z. Q. Tian, *Chem. Phys. Lett.* **1997**, *271*, 101.
[20] R. P. Van Duyne, J. C. Hulteen, D. A. Treichel, *J. Chem. Phys.* **1993**, *99*, 2101.
[21] C. Douketis, T. L. Haslett, Z. Wang, M. Moskovits, S. Iannotta, *J. Chem. Phys.* **2000**, *113*, 11315.
[22] R. P. Van Duyne, J. C. Hulteen, D. A. Treichel, *J. Chem. Phys.* **1993**, *99*, 2101.
[23] C.-D. Chen, Y.-T. Yeh, C. R. C. Wang, *J. Phys. Chem. Solids* **2001**, *62*, 1587.
[24] K. Siskova, B. Vlckova, P.-Y. Turpin, C. Fayet, *J. Phys. Chem. C* **2008**, *112*, 4435.
[25] D. Graham, W. E. Smith, A. M. T. Linacre, C. H. Munro, N. D. Watson, P. C. White, *Anal. Chem.* **1997**, *69*, 4703.
[26] C. H. Walker, J. V. St. John, P. Wisian-Neilson, *J. Am. Chem. Soc.* **2001**, *123*, 3846.
[27] A. C. Templeton, J. J. Pietron, R. W. Murray, P. Mulvaney, *J. Phys. Chem. B* **2000**, *104*, 564.
[28] R. M. Bright, M. D. Musick, M. J. Natan, *Langmuir* **1998**, *14*, 5701.
[29] N. Félidj, J. Aubard, G. Levi, J. R. Krenn, M. Salerno, G. Schider, B. Lamprecht, A. Leitner, F. R. Aussenegg, *Phys. Rev. B* **2002**, *65*, 075419.
[30] D. M. Kolb, R. Ullmann, T. Will, *Science* **1997**, *275*, 1097.
[31] T. R. Jensen, G. C. Schatz, R. P. Van Duyne, *J. Phys. Chem. B* **1999**, *103*, 2394.
[32] X. Zhang, M. A. Young, O. Lyandres, R. P. Van Duyne, *J. Am. Chem. Soc.* **2005**, *127*, 4484.
[33] B. Nikoobakht, M. A. El-Sayed, *J. Phys. Chem. A* **2003**, *107*, 3372.
[34] A. Tao, F. Kim, C. Hess, J. Goldberger, R. He, Y. Sun, Y. Xia, P. Yang, *Nano Lett.* **2003**, *3*, 1229.
[35] H. Masuda, K. Fukuda, *Science* **1995**, *268*, 1466.
[36] K. Nielsch, F. Muller, A. P. Li, U. Gosele, *Adv. Mater.* **2000**, *12*, 582.
[37] J.-L. Yao, J. Tang, D.-Y. Wu, D.-M. Sun, K.-H. Xue, B. Ren, B.-W. Mao, Z.-Q. Tian, *Surf. Sci.* **2002**, *514*, 108.
[38] V. G. Stoleru, E. Towe, *Microelectronic Eng.* **2005**, *81*, 358.
[39] J. L. Yao, G. P. Pan, K. H. Xue, D. Y. Wu, B. Ren, D. M. Sun, J. Tang, X. Xu, Z. Q. Tian, *Pure Appl. Chem.* **2000**, *72*, 221.
[40] B. L. Broglin, A. Andreu, N. Dhussa, J. A. Heath Jr, J. Gerst, B. Dudley, D. Holland, M. El-Kouedi, *Langmuir* **2007**, *23*, 4563.
[41] H. Ko, V. V. Tsukruk, *Small* **2008**, *4*, 1980.
[42] N. Ji, W. Ruan, C. Wang, Z. Lu, B. Zhao, *Langmuir* **2009**, *25*, 11869.
[43] R. J. Walsh, G. Chumanov, *Appl. Spectrosc.* **2001**, *55*, 1695.
[44] N. Pavenayotin, M. D. Stewart Jr, J. M. Valles Jr, A. Yin, J. M. Xu, *Appl. Phys. Lett.* **2005**, *87*, 193111.
[45] H. Lin, J. Mock, D. Smith, T. Gao, M. J. Sailor, *J. Phys. Chem. B* **2004**, *108*, 11654.
[46] A. Yu. Panarin, S. N. Terekhov, I. A. Khodasevich, P.-Y. Turpin, *Proc SPIE* **2007**, *6728*, 6728/1.
[47] S. N. Terekhov, A. Yu. Panarin, M. V. Parkhats, P. A. Apanasevich, I. A. Khodasevich, P.-Y. Turpin, V. S. Chirvony, in Conference Program of the LALS 2007, International Conference on Laser Applications in Life Sciences, Technical Digest, Moscow, Russia, **2007**, p. Tul04P1.
[48] A. Yu. Panarin, V. S. Chirvony, K. I. Kholostov, P.-Y. Turpin, S. N. Terekhov, *J. Appl. Spectrosc.* **2009**, *76*, 280.
[49] R. F. Pasternack, E. J. Gibbs, J. J. Vilafranca, *Biochemistry* **1983**, *22*, 2406.
[50] A. Huczko, *Appl. Phys. A: Mater. Sci. Process.* **2000**, *70*, 365.
[51] G. Wei, H. Zhou, Z. Liu, Z. Li, *Appl.Surf. Sci.* **2005**, *240*, 260.
[52] V. M. Shalaev, *Phys. Rep.* **1996**, *272*, 61.
[53] D. A. Genov, V. M. Shalaev, A. K. Sarychev, *Phys. Rev. B* **2005**, *72*, 113102.
[54] K. Seal, D. A. Genov, A. K. Sarychev, H. Noh, V. M. Shalaev, Z. C. Ying, X. Zhang, H. Cao, *Phys. Rev. Lett.* **2006**, *97*, 206103.
[55] Y. Yamamoto, N. Baba, S. Tajima, *Nature* **1981**, *289*, 572.
[56] T. Gao, G. Meng, L. Zhang, *J. Phys. Condens. Matter* **2003**, *15*, 2071.
[57] J. H. Chen, C. P. Huang, C. G. Chao, T. M. Chen, *Appl. Phys. A* **2006**, *84*, 297.
[58] O. K. Song, M. J. Yoon, D. Kim, *J. Raman Spectrosc.* **1989**, *20*, 739.
[59] N. Blom, J. Odo, K. Nakamoto, D. P. Strommen, *J. Phys. Chem.* **1986**, *90*, 2847.
[60] K. Bütje, K. Nakamoto, *J. Inorg. Chim. Acta* **1990**, *167*, 97.
[61] M. Moskovits, *J. Chem. Phys.* **1982**, *77*, 4408.
[62] A. Campion, P. Kambhampati, *Chem. Soc. Rev.* **1998**, *27*, 241.
[63] M. Moskovits, *J. Raman Spectrosc.* **2005**, *36*, 485.
[64] Z. Tai, J. Zhang, J. Gao, G. Xue, *J. Mater. Chem.* **1993**, *3*, 417.
[65] J. Qu, D. P. Arnold, P. M. Fredericks, *J. Raman Spectrosc.* **2000**, *31*, 469.